Hybrid Models of an Automotive Driveline*

Andrea Balluchi[†] Luca Benvenuti[§]
Claudio Lemma[†] Pierpaolo Murrieri[†]
Alberto L. Sangiovanni–Vincentelli[†¶]

[†] PARADES, Via di S.Pantaleo, 66, 00186 Roma, Italy.
{balluchi, clemma, murrieri, alberto}@parades.rm.cnr.it,

[§] DIS, Universitá di Roma La Sapienza, Via Eudossiana 18, 00184 Roma, Italy.
luca.benvenuti@uniroma1.it

[¶] Dept. of Electrical Engineering and Computer Sciences,
Univ. of California at Berkeley, CA 94720, USA.
alberto@eecs.berkeley.edu

February 25, 2005

Abstract

In this document, two hybrid models of an automotive driveline, differing in their levels of abstraction from real system behavior, are proposed. One model is very detailed, involves discrete dynamics with numerous states and its aim is to provide a powerful tool for verification. From the latter a reduced–order hybrid model, which is more indicated for synthesis purposes in the design of controllers/observers, is obtained analytically. Both hybrid models have been used with encouraging results within the research activity "*Hybrid algorithm development for the actual engaged gear identification in engine control application, simulation and experimental data processing*" developed by PARADES during the year 2004.

*This research has been sponsored by European Community Projects IST-2001-33520 CC (Control and Computation)

1 Introduction

To date, industry makes use in design flow of ever more detailed dynamical models with the aim to sensibly reduce onerous but inevitable verification–prototyping costs and times, preserving anyway the quality of its products. This is made possible by recently developments in description formalisms for dynamical systems that allow capturing behaviors of quite real phenomena.
Automotive follows this trend: car subsystems have been described with growing wealth of details and, consequently, involved dynamics grown in complexity. This is the reason why hybrid systems methodologies have been profitably used in modelling, analysis and control applications (see [6, 7]). For instance, in engine control a heterogenous and, to some extent, uncertain event–driven time domain is due to the behavior of the 4-stroke internal combustion engine. Indeed, driveline dynamics depends on some discrete conditions (i.e. stroke engine, backlash position) that can be represented as discrete components of the state, while transitions of the stroke engine and the backlash position are influenced by the continuous state evolution.
From a control–designer point of view, completeness of plant models is often paid with unacceptable difficulties in controllers design. This is the reason why models should be provided with different levels of details. In this document a detailed hybrid model of a car driveline for verification purposes and a reduced–order hybrid model useful for controller synthesis are developed. Equations describing the two lumped parameters models are derived from the second law of dynamics. This is a good approximation even if parameters strongly depend from temperature and frequency, and transmission axis are deformable continuous bodies (when one of the axis is too long more detailed distributed–parameters models can be found in [10]). To be a useful verification tool, the developed hybrid model:

– represents dynamics of the driveline for every engaged gear and in every discrete state of the clutch;

– represents the transitory when it is switched from one discrete state to the other;

– predicts the continuous and discrete state of the driveline with high precision;

– the detailed hybrid model represents a great number of discrete states (6048) and has 12 variables of continuous state.

On the contrary, to be extremely effective for controllers/observers synthesis, the developed reduced–order hybrid model:

– represents the driveline as a third order linear system when the clutch is close. So, we have a compact, manageable and low computational expensive representation of the driveline;

– represents the basic oscillations of the driveline when the engaged gear is varying;

– allows to simulate the gear shifting.

Both detailed and simplified models have been developed by PARADES GEIE during the year 2004 in collaboration with Magneti Marelli Powertrain within the research activities: "*Hybrid algorithm development for the actual engaged gear identification in engine control application, simulation and experimental data processing*" (see [5]). Effectiveness of the detailed hybrid model for verification has been confirmed by experimental data.
In Section 1.1, 1.2, 1.3, notions on the use of the gear–box, the driveability and the control of the driveline are provided. In Section 2, 3, the detailed hybrid model is described and a comparison between simulated and experimental data is reported. In Section 4, the reduced–order hybrid model is developed and the comparison with the detailed hybrid model is illustrated.

1.1 Gear–box: why?

To encounter customers' satisfactory specifications and comply with tight law restrictions, current engines must have optimal performances for a wide range of speeds and loads with acceptable fuel consumptions and high quality of exhaust gas.
A constant power with respect to speed is favorable since, in this case, the curve

$$P = F_{opt} v \tag{1}$$

yields a traction force F_{opt} that is hyperbolic with respect to speed (its points are stable). Unfortunately, a typical torque curve of a real IC engine is not hyperbolic, see Figure 1. In particular, the torque curve has a maximum point that divides the set of stable points from unstable ones. For this reason, a single fixed gear ratio, which connects the engine to the wheels, is advised and it is necessary to introduce a device that reshapes the torque curve. Figure 2 depicts the transformations, introduced by a manual gear–box with four gears, on the torque curve. It is worthwhile to note that better approximations of the traction force F_{opt} are achieved by gear–box with a high number of gears.

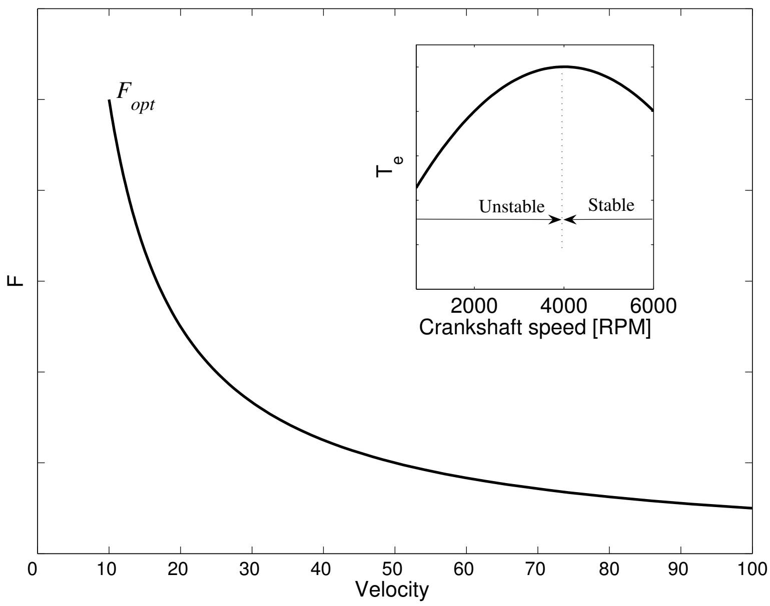

Figure 1: Optimal power curve and torque curve of a generic IC engine.

1.2 Driveability

Driveability collects many drive comfort factors: it is related to the subjective perception of the driver and represents a very important factor for the commercial success of a product. Since it is strongly influenced by the behavior of the vehicle during transient conditions, driveability is typically evaluated in acceleration, gear shifting, engine start behavior, idle, braking, shunt and shuffle.

Moreover, it is very difficult to capture the subjective feeling of the driver in a single quantitative mark. Therefore, automotive producers followed a statistical approach making extensive series of tests with expert drivers who attribute a driveability mark using a scale from 1 to 10 (see Table 1). Since this step in the production chain is costly either in terms of time and money, then it is important to have detailed models of the driveline and evaluate on these the driveability. For instance, in [14, 15] Johansson *et al.* define some indices in order to indicate the degree of shuffle and shunt using the FFT, VDV and differences in acceleration values, see [13]. In [14, 15] a literature survey on the driveability is reported.

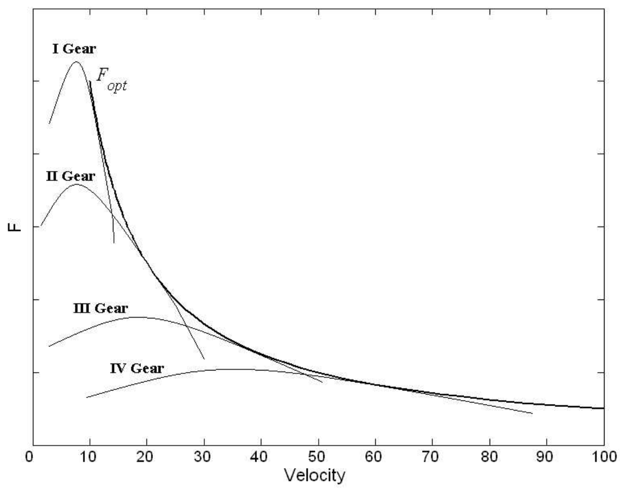

Figure 2: Approximation of the optimal–power curve using a gear–box with four gears.

1.3 Driveline control scenario

The driveline is the set of mechanical devices that transmit the engine torque to wheels. For this reason its dynamics influences remarkably the drive comfort and driveability of the car.
Since the driveline contains elastic elements, then fastidious oscillations and jerk effects occur especially during transients, such as tip–in, tip–out and gear shifting actions[1]. During tip–in and tip–out the following phenomena are distinguished (see Figure 3):

***shunt*:** is an initial jerk that might occur during a rapid change in vehicle acceleration (some backlash might hit the other side and be cause of sharp derivative on the acceleration);

***shuffle*:** is the longitudinal oscillation of the vehicle excited by the torsional oscillation of the driveline;

***clonk*:** is the sound during the shunt and shuffle period. It is a high frequency, metallic noise, occurring when two shafts, between which there is a backlash, bump one against the other. The clonk duration is varying from 0.25 to 5 ms (see [21]).

[1]Tip–in and tip–out correspond to sudden positive or negative respectively actions on the throttle pedal.

Driveability mark	Subjective description	Corresponding comment
10	Excellent	Not noticeable even by experienced drivers
9	Very good	Disturbing for experienced drivers
8	Good	Disturbing for critical customers
7	Satisfying	Disturbing for several customers
6	Even satisfying	Disturbing for all customers
5	Adequate	Very disturbing for all customers
4	Defective	Felt to be deficient by all customers
3	Insufficient	Reclaimed as deficient by all customers
2	Bad	Limited vehicle operating only
1	Very bad	Vehicle not operating

Table 1: Standard rating scale for driveability.

The parameters that mostly influence shunt and shuffle are:

- the length of the backlash;
- the elasticity of the axis of transmission, the clutch springs and the engine suspensions;
- the engaged gear.

Shunt and shuffle are perceived from the passengers as an unpleasant longitudinal oscillations. The human body well tolerates vertical oscillations of the vehicle since it perceives them as walking. On the contrary, horizontal oscillations are remarkably unpleasant. Since mechanical resonance frequencies of the human body organs are approximately $4-6$ Hz for shoulders, $4-8$ Hz for stomach and $3-6$ Hz for the upper trunk (see [13]), and driveline natural frequency is comprised between $1-10$ Hz, then controlling the longitudinal oscillations becomes important to improve comfort and driveability. The problem of the shunt and shuffle was introduced in the 80s. In the wide literature two strategies are mainly suggested:

- preventing shunt and shuffle by mechanical construction;
- accepting the existence of shunt and shuffle and reducing them by control[2] (see [2, 17, 18, 18, 22, 25, 28, 29, 32, 34]). For instance, shunt can be reduced by appropriate control laws when the engine troughs a backlash. In this way, when the backlash changes direction, the bump impulse is reduced. Besides, shuffle reduction problem can be approached with:

[2]In this case the engine is seen as an actuator.

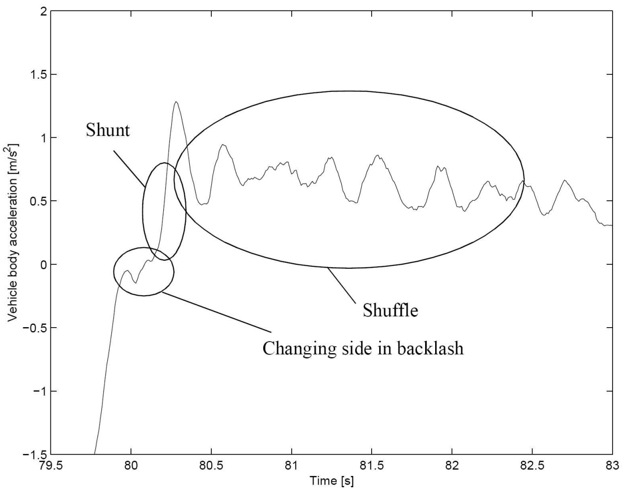

Figure 3: Vehicle body acceleration during a tip-in in a typical car, reported in [16].

a) a low-pass filter on the requested torque. In this way, the oscillations are reduced but, at the same time, the performances of the engine are limited.

b) active control of the torque engine in order to damp oscillations.

Other disturbances, the *rattle* and the *clatter* (see [3, 9, 20]), are acoustic and generated by the bounce of the mechanical axis inside the backlash area because of vibrations on the pulsating torque engine. While the clonk is generated from the abrupt impact between axes during tip–in or tip–out, the rattle and the clatter are generated by the impact of the axes when the transmitted torque is close to zero. For instance, gear-box produces rattle in neutral and clutter with an engaged gear. Normally the rattle and the clutter are limited by a good acoustic isolation, by an opportune construction of the gears and by a damping/springs system on the clutch or on the flywheel.

As previously stated (see Section 1.1), introducing the gear–box is necessary in order to efficiently couple engine and wheels. However, a frequent use of clutch pedal and gear lever of a conventional manual gear–box can tire the driver. The conventional automatic gear–box (CVT) solves this problem but, at the same time, it involves additional costs, torque losses, greater mechanical complexity and shorter life cycle (especially when used on tracks). In the last years, performances were improved by the robotized gear–box that is mechanically identical to the manual gear–box but has a controller for the clutch and the gear lever. A control scenario for the robotized gear–box

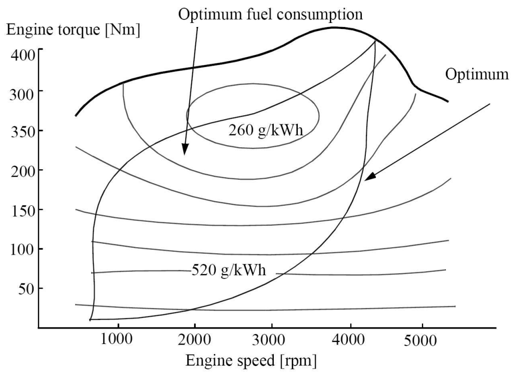

Figure 4: Performance map for a typical Otto engine (see [16]).

concerns:

- an automatic control of the clutch and manual gear lever. Of particular interest is the vehicle start-up from stop (launch control) (see [11, 23, 30]);
- an automatic control of the gear lever and manual clutch;
- an automatic control of the clutch and of the gear lever (see [24, 25, 26]).

In particular, latter task has been mainly achieved by:

- the use of the clutch during the gear shifting. It is necessary to manage the following steps: decouple the clutch, engage the neutral, engage the new gear, couple the clutch;
- shifting the gear without the use of the clutch. It is necessary to manage the following steps: control the transmitted torque to zero, engage the neutral, carry the speed engine at the transmission speed (scaled with the conversion ratio of the new gear), engage the new gear. The critical step in this gear shifting strategy is to control the torque to zero. In this case, the driveline oscillations limit considerably the minimum time for the gear shifting: in fact, until the oscillations are not damped, it is not possible to insert neutral gear.

The right gear–shifting control can considerably improve the fuel consumption, the exhaust–gas emissions, the driveability and the performances. The iso–consumption curves of the torque–speed plan are depicted in Figure 4, along with the optimal–fuel–consumption and performances lines. The picture evidences that different sequences of controls for the same gear shift produce either optimal fuel consumptions or optimal performances.

2 The detailed driveline hybrid model $\mathcal{H}_M$

In this section a detailed hybrid model $\mathcal{H}_M$ of the driveline is described. The configuration of the driveline and the total number of axes involved depend on the relative position between the engine and the actuated wheels. Indeed, the engine can be arranged longitudinally or transversely with respect to forward velocity direction, in a front or rear position of the car; the actuated wheels can be frontal, rear or both. In this document it is referred to a car with both the engine and the actuated wheels arranged in a front, and the engine put transversally.

Figure 5 depicts a synthetic scheme of the model $\mathcal{H}_M$ with crankshaft, flywheel, clutch, gear–box, cylinder block, semi–axle, wheel group, tire and chassis dynamics put in evidence. Notice that the contributions to dynamics of the couple of semi–axes and tires are not treated separately but collected in an unique equivalent system. Exogenous continuous inputs are the engine average torque T_e, the engine temperature t_{engine}, the torque T_{brake} produced by the braking system, the torque T_{slope} due to the slope of the road, the aerodynamics friction torque T_{air} and the clutch pressure P_{clutch}. The only exogenous discrete input is the position of the gear lever. The following

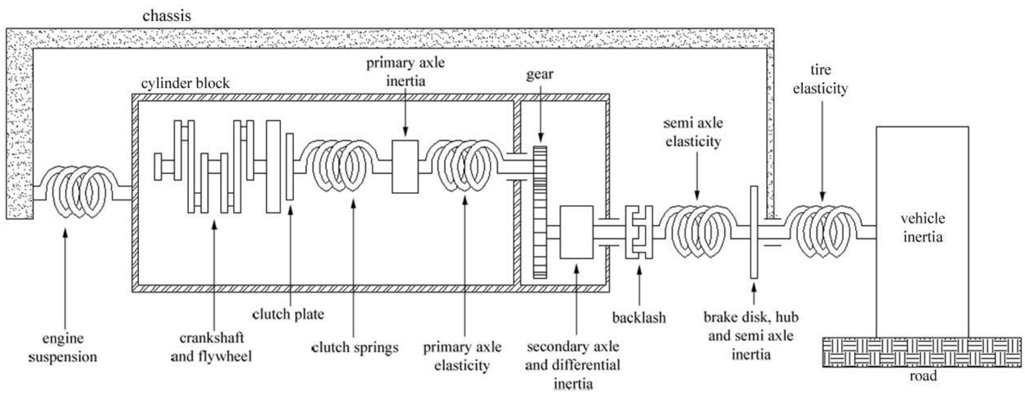

Figure 5: Scheme of the detailed hybrid model $\mathcal{H}_M$.

subsections provide a description of each subsystem involved in the driveline model.

2.1 Crankshaft and flywheel model.

The crankshaft and the flywheel are modelled as an unique first–order continuous–time system (from here referred to as crankshaft) characterized by an overall inertia J_e that collects the contributions of the connecting rods, pistons, valve train system, alternator and any other auxiliary device rigidly connected to the crankshaft[3]. Input torques for the crankshaft dynamics are the engine torque T_e, the friction torque T_{fric} and the clutch coupling torque T_{clutch}, that yields

$$T_e = J_e\dot{\omega}_e + T_{fric}(\omega_e, t_{engine}) + T_{clutch}, \tag{2}$$

where ω_e is the crankshaft angular velocity.

The torque T_{fric} is mainly due to pumping losses and bearing frictions;

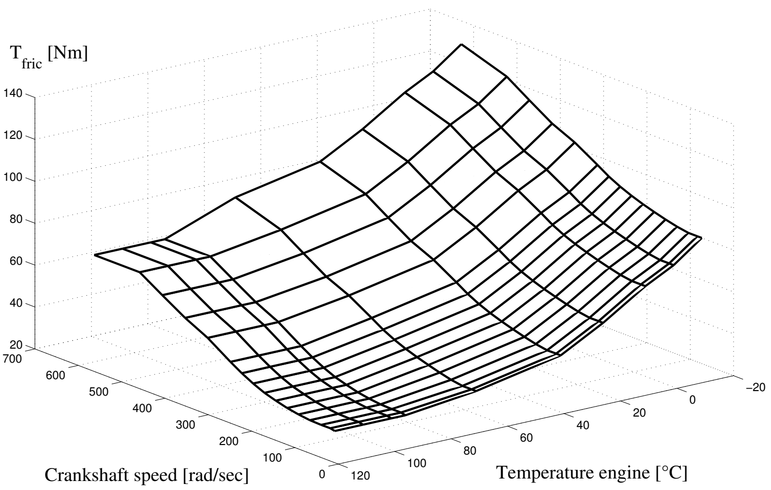

Figure 6: Torque friction on the crankshaft.

it collects the contributions of valve–train system, oil pump and auxiliary devices loads (power steering, alternator, air conditioner, etc..., see [1]). The friction torque T_{fric} has a nonlinear behavior with respect to engine speed and temperature[4]. It is modelled by the look–up table of Figure 6.

[3]The inertia of the single auxiliary device can be small if compared to the crankshaft and the flywheel inertias. Nevertheless, the contribution of these inertias can not be neglected because the auxiliary devices are coupled to the crankshaft with a mechanical ratio that can be appreciable (about 2.5).

[4]Friction concerns viscously coupled mechanical components and the medium viscosity itself is function of the temperature.

In the last years an alternative to the conventional flywheel is represented by the *dual mass flywheel* (DMF), that is frequently mounted on vehicles with wide Diesel motorization (see [8, 27]). This solution has improved driveability, comfort and fuel consumption. Indeed, since the cyclic combustion process in IC engines is the main source of vibrations for the driveline, then springs/damping systems are mounted on the clutch plate, acting as mechanical low–pass filters with cut frequencies smaller than the idle speed. Nevertheless, at low engine speed, vibrations are still perceptible from drivers. The dual mass flywheel is composed by a rigid clutch plate and two masses connected by a springs/damping system. It is mounted so that the inertia on the engine side is dynamically reduced while that on the transmission side is increased. The effect is perceived as drastically reduced driveline oscillations. Hence, the drive becomes comfortable also for low speeds where the fuel specific consumption is smaller (see Figure 4), especially in the Diesel engines that have a flat torque curve. In Figure 7 it is depicted a static characteristic

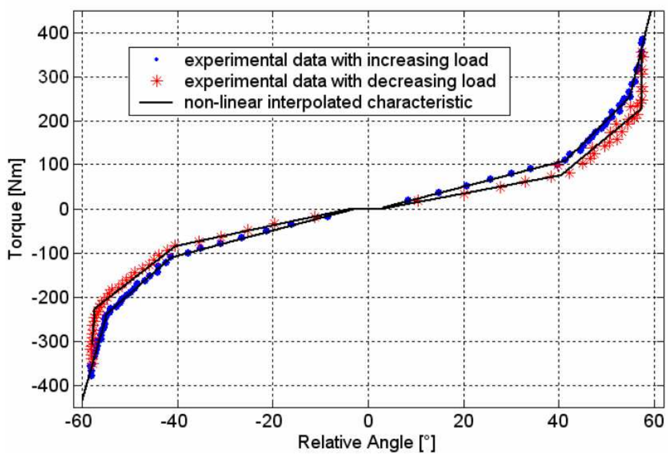

Figure 7: DMF springs static characteristic, either measured and interpolated [8].

of the dual mass flywheel obtained in experimental setups. To simplify the model presented in this document, a conventional flywheel is addressed since the insertion of a dual mass flywheel can be easily derived from the example in Section 2.2, 2.3 and Figure 7.

2.2 Clutch plate model.

The clutch is modelled as a hybrid system with three discrete states: *Close, Slip* and *Open* (see Figure 8).

In the discrete state *Close*, the clutch plate and the flywheel are rigidly

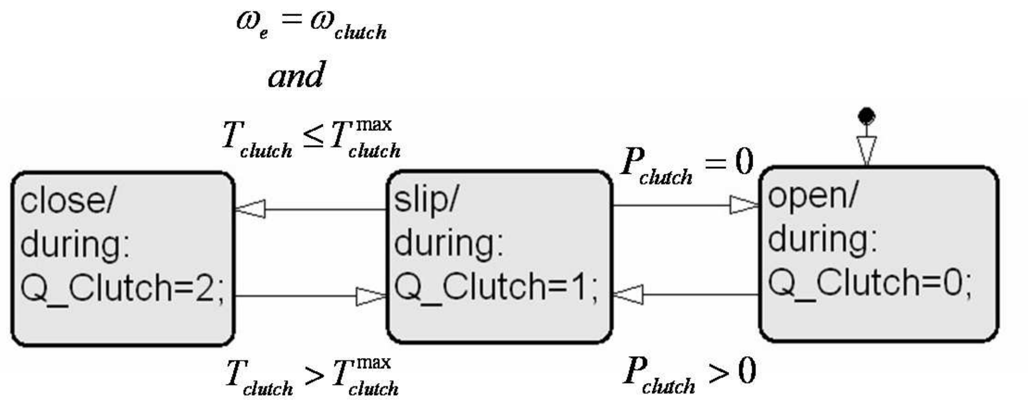

Figure 8: Clutch FSM.

connected by static friction, so that their inertias are merged in a single first–order system. The maximal static friction torque T_{clutch}^{max} that can be transmitted before incurring in clutch slippage is a function of its size and pressure P_{clutch}, i.e.

$$T_{clutch}^{max} = \mu_s n_s \frac{2\pi}{3} \frac{R_{ext}^3 - R_{int}^3}{3} P_{clutch}, \tag{3}$$

while the torque transmitted by the clutch is

$$T_{clutch} = (T_e - T_{fric}) \frac{J_{clutch}}{J_{clutch} + J_e} + T_{springs} \frac{J_e}{J_{clutch} + J_e}. \tag{4}$$

When $T_{clutch} > T_{clutch}^{max}$ the clutch model enters in the state *Slip*: the clutch plate and the flywheel are not more a rigid body but they slip one on the other. In this case the coupling torque is

$$T_{clutch} = \mu_d(\omega_e - \omega_{clutch}) n_s \frac{2\pi}{3} \frac{R_{ext}^3 - R_{int}^3}{3} P_{clutch} sign(\omega_e - \omega_{clutch}), \tag{5}$$

where the coefficient of kinematic friction $\mu_d(\cdot)$ is function of the slipping speed $\omega_e - \omega_{clutch}$ as reported in Figure 9.

If $\omega_e = \omega_{clutch}$ and $T_{clutch} \leq T_{clutch}^{max}$, then the clutch model returns in the

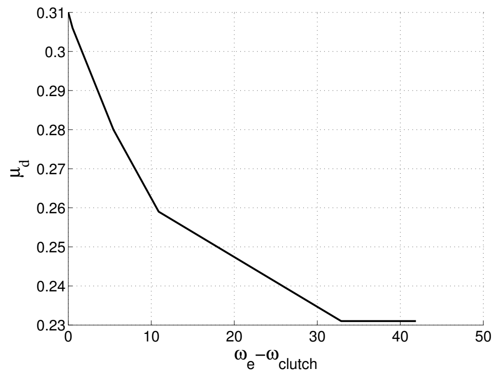

Figure 9: Coefficient of kinematic friction μ_d.

state *Close*. If $P_{clutch} = 0$ it enters, instead, in the state *Open* and the transmitted torque is zero, i.e. $T_{clutch} = 0$. In the state *Open* the crankshaft is completely decoupled from the rest of the driveline and the two systems follow independent dynamics.
For simplicity sake, nonlinear terms in T_{clutch}, which are function of P_{clutch} and temperature, are neglected in (3) and (5).
In any case, for any coupling torque, the clutch plate dynamics is:

$$T_{clutch} - T_{springs} = J_{clutch}\dot{\omega}_{clutch}. \tag{6}$$

2.3 Clutch springs model.

As previously stated, see Section 2.1, a springs/damping system is mounted on the clutch plate in off-the–shelf drivelines, in order to limit vibrations due to engine pulsating torques. This system connects the clutch plate with the primary axle of the gear–box, allows sweet engagements of the clutch, and avoids fastidious jerks. The nonlinear static torsion–torque characteristic of the clutch springs is depicted in Figure 10. For increasing values of the torsion angle, a growing number of pre–charged springs act on the axle, so that the piecewise linear characteristic of Figure 10 is obtained. When the maximum excursion of the torsion angle is obtained, a mechanical stop makes the coupling rigid.

To capture the piecewise linear characteristic, clutch springs dynamics is modelled by a hybrid system with eight discrete states, see Figure 11, where each state represents a linear segment of the characteristic in Figure 10. In

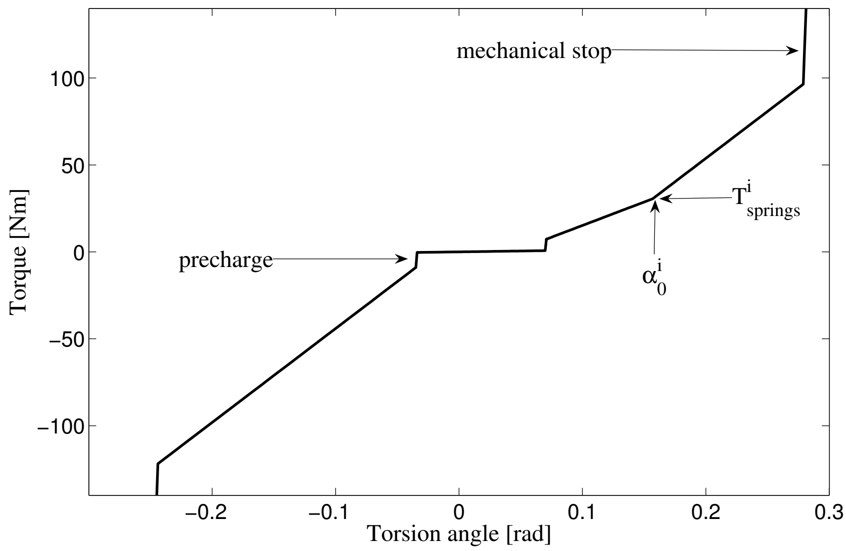

Figure 10: Clutch springs static characteristic.

the i-th discrete state, the transmitted torque $T_{springs}$ is described by:

$$\begin{aligned}\dot{\alpha}_{springs} &= \omega_{clutch} - \omega_p \\ T_{springs} &= K_{fi}(\alpha_{springs} - \alpha_0^i) + B_{fi}(\omega_{clutch} - \omega_p) + T^i_{springs}.\end{aligned} \tag{7}$$

2.4 Cylinder block model.

The cylinder block is connected to the chassis of the car by suspensions and revolves approximately on a spindle that is coincident with the semi–axle. The cylinder block is subject to the engine suspensions torque T_{susp} and the reaction torque $-T_{sma}$ from semi–axle subsystem, so that its dynamics is:

$$T_{susp} - T_{sma} = J_b \dot{\omega}_b. \tag{8}$$

The static torque–torsion characteristic of engine–suspensions coupled system is nonlinear and similar to the clutch–springs one of section 2.3. Hence, the engine suspensions dynamics is described by the 8–states hybrid model depicted in Figure 12. The Figure depicts also the static torque–torsion

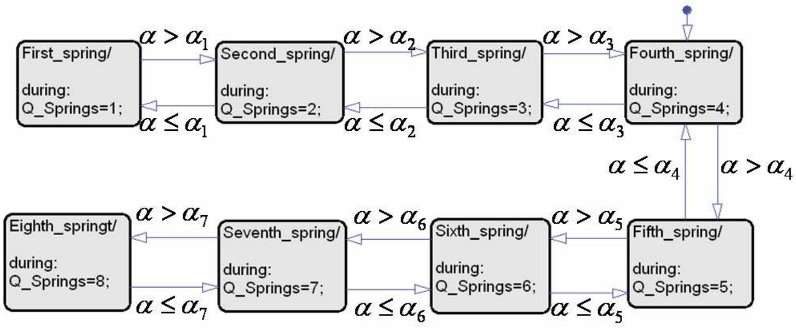

Figure 11: Clutch springs FSM.

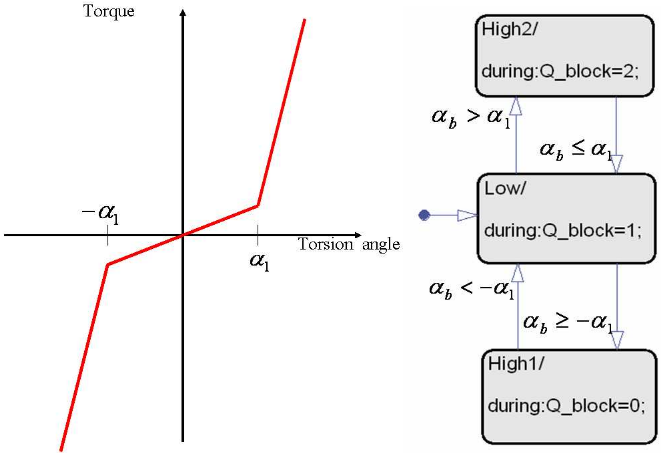

Figure 12: Static characteristic of torsion (left) and FSM of cylinder block (right).

characteristic. The torque T_{susp} is defined by:

$$\begin{aligned} \dot{\alpha}_b &= \omega_b \\ T_{susp} &= \begin{cases} k_{low}\alpha_b + B_{low}\omega_b & \alpha_b \in [-\alpha_1, \alpha_1] \quad Low \\ k_{high}(\alpha_b - \alpha_1) + k_{low}\alpha_1 + B_{high}\omega_b & \alpha_b > \alpha_1 \quad High2 \\ k_{high}(\alpha_b + \alpha_1) - k_{low}\alpha_1 + B_{high}\omega_b & \alpha_b < -\alpha_1 \quad High1 \end{cases} \end{aligned} \tag{9}$$

2.5 Gear–box model.

The gear–box is modelled as a hybrid system with seven discrete states (see Figure 13): one for each forward and reverse gear, one for neutral. The gear–box automaton switches from one discrete state to another in function

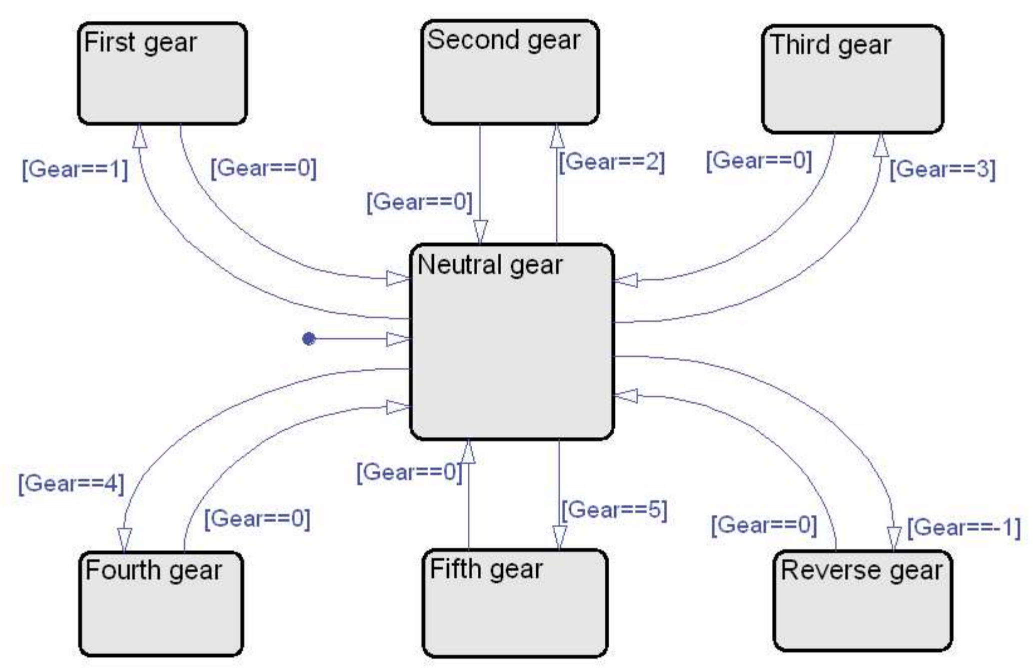

Figure 13: Gear–box FSM.

of *Gear* signal which is synchronous with command–lever position. It is worthwhile to recall that *Gear* is the only discrete input exogenous to the whole hybrid system.
Notice that the FSM depicted in Figure 13 has a sequential behavior as the conventional manual gear–boxes.
The gear–box continuous part comprises[5]

- the primary axle with inertia J_p and elasticity coefficient k_p, collecting also the elasticity of the secondary axle and of the differential that is assumed to be constant[6];
- one rigid inertia that collects the secondary axle and the differential.

[5] In the gear–box hybrid model we have not modelled the synchronizer.

[6] This is an approximation because the total elasticity of the gear–box depends on the engaged gear and transmission ratio τ_i.

When the i-th gear is engaged, the continuous state has the dynamics

$$\begin{aligned}
\dot{\alpha}_p &= \omega_p - \tau_i \tau_{diff} (\omega_{diff} - \omega_b) \\
T_{springs} &= J_p \dot{\omega}_p + B_p \omega_p + k_p \alpha_p \\
&\quad + B_{ps} \big(\omega_p - \tau_i \tau_{diff} (\omega_{diff} - \omega_b) \big) \\
\hat{J} \dot{\omega}_{diff} + \hat{B} \omega_{diff} + T_{sma} &= \frac{1}{\tau_i \tau_{diff}} \big[k_p \alpha_p + B_{ps} \big(\omega_p \\
&\quad - \tau_i \tau_{diff} (\omega_{diff} - \omega_b) \big) \big],
\end{aligned} \tag{10}$$

where

$$\hat{J} = \frac{J_s}{\tau_{diff}^2} + J_d; \quad \hat{B} = \frac{B_s}{\tau_{diff}^2} + B_d. \tag{11}$$

When the neutral gear is engaged, the primary and secondary axles are completely decoupled and follow independent dynamics, i.e.

$$\begin{aligned}
\dot{\alpha}_p &= -1 \\
T_{springs} &= J_p \dot{\omega}_p + B_p \omega_p \\
\hat{J} \dot{\omega}_{diff} + \hat{B} \omega_{diff} + T_{sma} &= 0.
\end{aligned} \tag{12}$$

2.6 Semi-axle and backlash model.

In the driveline a small backlash is present in all mechanical connections: between clutch and primary axle, primary and secondary axes, secondary axle and differential, differential and semi–axle, semi–axle and hub, and inside the differential on the satellites–planetariums system and synchronizer. The sum of these small backlashes produces, however, a great dead zone on the driveline that is quite wide $30 - 40$ degrees at the crankshaft.
The semi–axes are very elastic and connect the differential to the hub. Because of their elevated elasticity the semi–axes are an important center of torsional energy in the driveline. In the semi-axes, besides torsional oscillations, are also presented longitudinal oscillations that are unpleasantly perceived from the passengers. In order to dump the longitudinal oscillations several solutions exist. For instance, it is possible to damp the longitudinal oscillations by adding a lumped inertia on a intermediate point of the semi–axis. In common operating modes longitudinal oscillations are small and, hence, are neglected in the model $\mathcal{H}_M$.
For the sake of simplicity, an unique backlash is connected to the semi–axle and the inertia of the semi–axle is attributed to the hub. The equivalent elasticity of the single semi–axle is:

$$k_{sma} = \frac{4 k_l k_r}{k_l + k_r}. \tag{13}$$

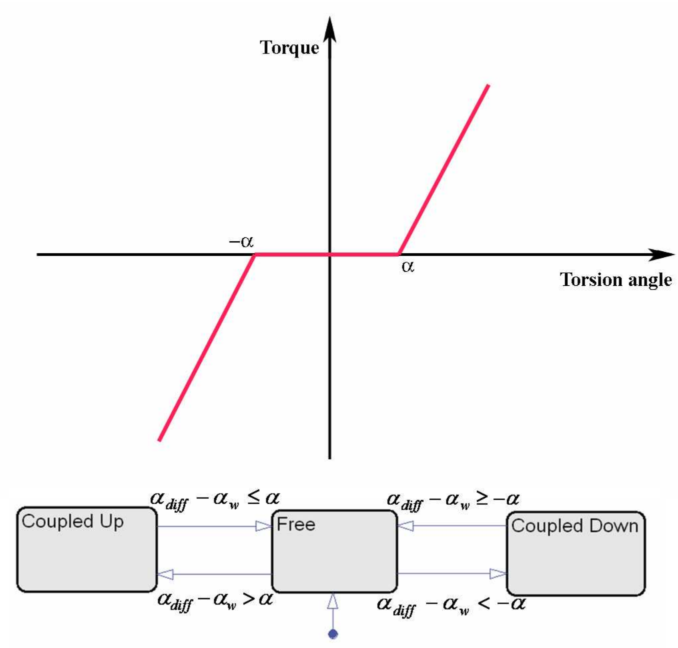

Figure 14: Static torsion characteristic of the semi–axle with backlash (top) and FSM of the hybrid model (bottom).

The static torsion characteristic of the semi–axle with backlash is depicted in Figure 14. As done for engine suspensions in Section 2.4, the semi–axle with backlash is modelled as a hybrid system with three discrete states whose FSM is reported in Figure 14. When $|\alpha_{diff} - \alpha_w| \leq \alpha$ the discrete state *Free* is entered, the differential is completely decoupled from the hub and the transmitted torque T_{sma} is:

$$T_{sma} = 0. \tag{14}$$

When the backlash is null, for $(\alpha_{diff} - \alpha_w) > \alpha$, the differential is connected to the hub by the elasticity of the semi-axle and the discrete state *Coupled–Up* is entered. In this case, the T_{sma} is:

$$T_{sma} = k_{sma}(\alpha_{diff} - \alpha_w - \alpha) + b_{sma}(\omega_{diff} - \omega_w). \tag{15}$$

When $(\alpha_{diff} - \alpha_w) < -\alpha$ the discrete state *Coupled–Down* is entered and the T_{sma} is:

$$T_{sma} = k_{sma}(\alpha_{diff} - \alpha_w + \alpha) + b_{sma}(\omega_{diff} - \omega_w). \tag{16}$$

In any case, the angles α_{diff}, α_w are

$$\begin{aligned} \dot{\alpha}_{diff} &= \omega_{diff} \\ \dot{\alpha}_w &= \omega_w \end{aligned} \tag{17}$$

2.7 Wheel group model.

With the term *wheel group* we denote the wheel disc, the semi–axle inertia[7], the hub, the disc brake and the tire. The hub is a short axle that revolves inside a support connected to the chassis by a shock-absorber. On one side of the hub there is connected the semi–axle while, on the other, the wheel and the disc brake. The following torques act on the wheels group: the torque T_{brake} of the brake system, the viscous linear friction $b_w\omega_w$ of the hub bearing, the torque T_{sma} transmitted by the semi–axle and the torque $\hat{T}_{tire}$ transmitted by the tire. The wheel group follows the dynamics

$$T_{sma} - T_{brake} - \hat{T}_{tire} = J_w\dot{\omega}_w + b_w\omega_w. \tag{18}$$

The tire has the experimental nonlinear static characteristic represented in Figure 15 where, in particular, a hysteresis phenomenon is evident. The hysteresis is modelled as a hybrid system with five discrete states whose FSM is depicted in Figure 16. In Figure 17 the static characteristic of torsion of the tire hybrid model is reported. In order to understand the hysteresis model, the reader must think to a cycle in which the tire, initially stopped, is twisted cyclically in the two spin directions. The angle of torsion of the tire is:

$$\dot{\alpha}_{tire} = \omega_w - \omega_{vehicle}. \tag{19}$$

After a positive torsion of the tire, that is initially stopped, the FSM enters the discrete state *Start* and the tire behaves as a spring with an elasticity k_{hyst}. When the torsion angle exceeds $\alpha_l/2$ the FSM enters the discrete state *One* and the elasticity becomes k_{lin}, with $k_{lin} < k_{hyst}$. If the torsion direction is inverted, the FSM enters in discrete state *Two* and the elasticity returns to the value k_{hyst}. When the torsion angle exceeds $-\alpha_l$, then the FSM switches to the discrete state *Three* with the elasticity k_{lin}. Changing newly torsion direction, the FSM enters the discrete state *Four* with elasticity k_{hyst}. The torque transmitted by the tire is:

- in the discrete state *Start*:

$$\hat{T}_{tire} = k_{hyst}\alpha_{tire} + b_t(\omega_w - \omega_{vehicle}); \tag{20}$$

[7]The semi–axle is modelled as a mass–dump–spring system whose inertia is added to wheel group while its elasticity has been modelled in the previous section.

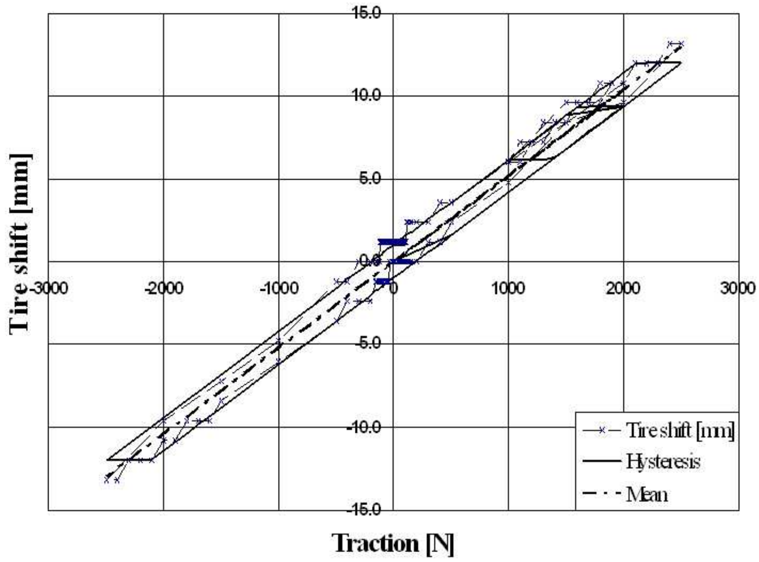

Figure 15: Experimental static torsion characteristic of a tire.

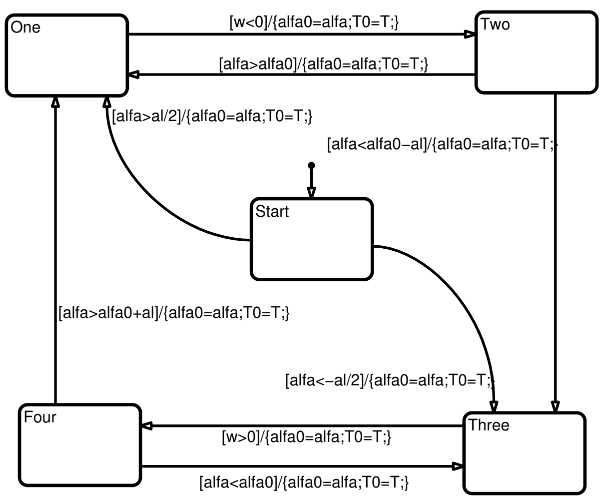

Figure 16: FSM of tire hybrid model.

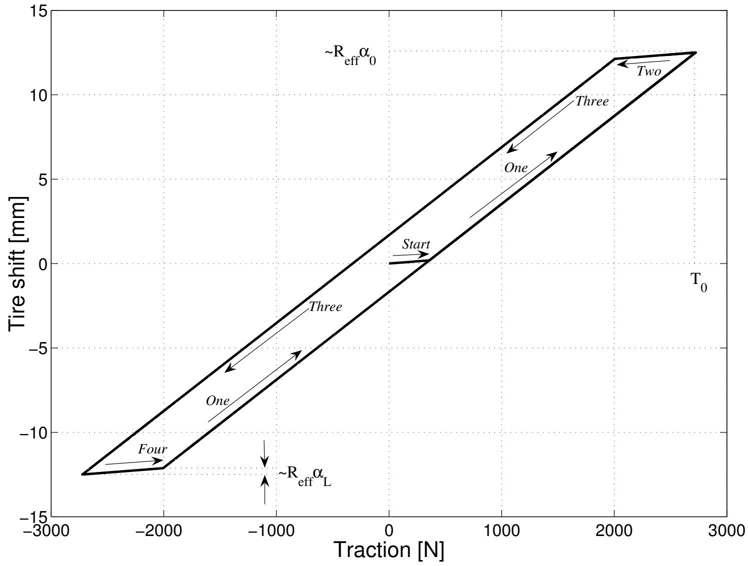

Figure 17: Static torsion characteristic of tire hybrid model.

- in *One* and *Three*:

$$\hat{T}_{tire} = k_{hyst}(\alpha_{tire} - \alpha_0) + T_0 + b_t(\omega_w - \omega_{vehicle}); \tag{21}$$

- in *Two* and *Four*:

$$\hat{T}_{tire} = k_{lin}(\alpha_{tire} - \alpha_0) + T_0 + b_t(\omega_w - \omega_{vehicle}). \tag{22}$$

The tire transmits a torque $\hat{T}_{tire}$ to the hub and the torque

$$T_{tire} = \hat{T}_{tire} - T_{roll}, \tag{23}$$

to the vehicle, with T_{roll} the rolling friction of the tire. Notice that T_{roll} is zero for $\omega_{vehicle} = 0$, while for $\omega_{vehicle} \neq 0$ $T_{roll} = Constant \cdot sign(\omega_{vehicle})$[8].

2.8 Vehicle body model.

The vehicle body is modelled by a first order dynamical system with inertia J_v and inputs: the torque T_{tire} transmitted by the tire, the torque T_{slope} due

[8] T_{roll} and R_{eff} depend on the mass of the vehicle, on the acceleration on the three cartesian axes and on the vehicle speed. In this document they are assumed constants.

to the slope of the road and the aerodynamics friction T_{air} (see [4, 12]). The dynamics of the vehicle is:

$$T_{tire} - T_{slope} - T_{air} = J_v \dot{\omega}_{vehicle}, \tag{24}$$

where[7]:

$$J_v = M_v R_{eff}^2. \tag{25}$$

The T_{slope} torque depends on the road slope $P_{\%}$, i.e.

$$T_{slope} = g M_v R_{eff} P_{\%}. \tag{26}$$

The T_{air} is:

$$T_{air} = 0.5 \rho C_x A R_{eff} (R_{eff} \omega_{vehicle})^2 sign(\omega_{vehicle}) \tag{27}$$

3 Detailed hybrid model simulations.

In this section, by comparing simulation results to experimental data, the effectiveness of the hybrid model $\mathcal{H}_M$ is shown.

– In Figure 3 (A), the elastic torsional characteristic of the driveline model $\mathcal{H}_M$ is compared with experimental data. As the figure makes clear, the model is able to represent the hysteresis of the characteristic, due to the tires, and the discontinuity of the elastic coefficient due to the engine suspensions and backlashes.

– Figure 3 (B) depicts the simulated acceleration of the car during a tip–in. It is possible to recognize a shunt at the begin and the successive shuffle as in Figure. 3.

– Figures 3 (C) and (D) depict the temporal evolutions of the crankshaft speed of the hybrid model $\mathcal{H}_M$ (C) and of a real car (D) during a tip–out followed by a tip–in.

– Figures 3 (E) and (F) depict the crankshaft speed and the discrete state of the clutch of the hybrid model $\mathcal{H}_M$ (E) and of a real car (F) during the vehicle start-up from to stop. The discrete state of the clutch assumes the values 0, 1, 2 with the following meaning:

1 clutch *Open*

2 clutch *Slip*

3 clutch *Close*

In the experimental data the state *Slip* is merged in the state *Open*.

– Figures 3 (G) and (H) depict the crankshaft speed and the discrete state of the clutch of the hybrid model $\mathcal{H}_M$ (G) and of a real car (H) during a gear shifting from the first to the second gear.

One important verification of the clutch is to study the power conservation (see Figure 19). The principle of conservation of the energy yields:

$$P_{in} = P_{out} \tag{28}$$

where:

$$\begin{aligned}
P_{in} &= (T_e - T_{fric})\omega_e \\
P_{out} &= P_{J_e} + P_{J_{clutch}} + P_{springs} \\
P_{J_e} &= J_e \dot{\omega}_e \omega_e \\
P_{J_{clutch}} &= J_{clutch} \dot{\omega}_{clutch} \omega_{clutch} \\
P_{springs} &= T_{springs} \omega_{clutch}
\end{aligned}$$

In Figure 19 it is depicted with a continuous line the P_{in} and with a dash line the P_{out} during a start-up from to stop in first gear of the vehicle. When the clutch is in the state *Open* and *Close*, a perfect balance of the power is held: part of the power P_{in} accelerates the inertias J_e and J_{clutch} and the remaining amount is transmitted to the gear–box. During the state *Slip*, instead, a part of the power is lost in thermal energy P_{th}.

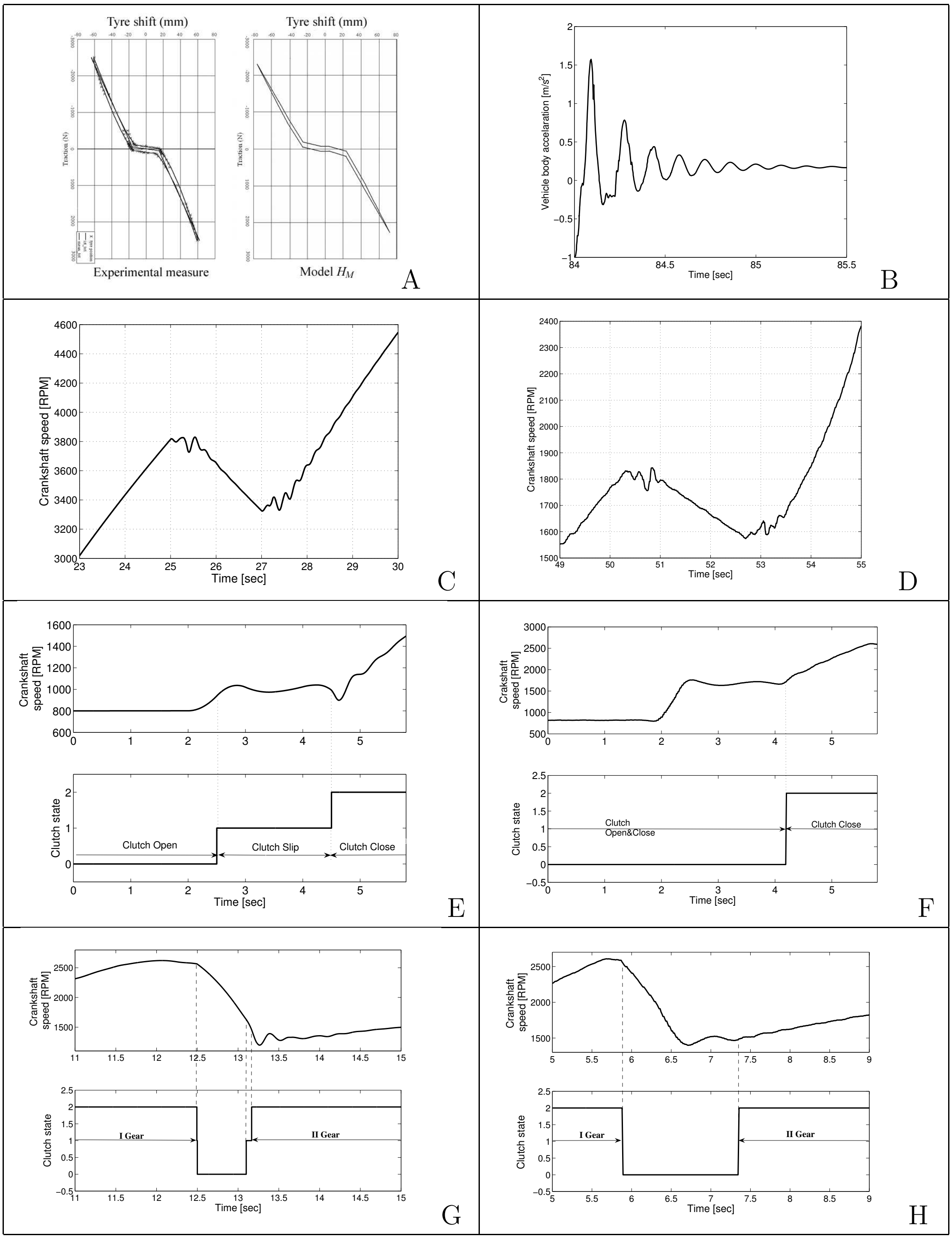

Figure 18: Comparison between simulations and experimental data.

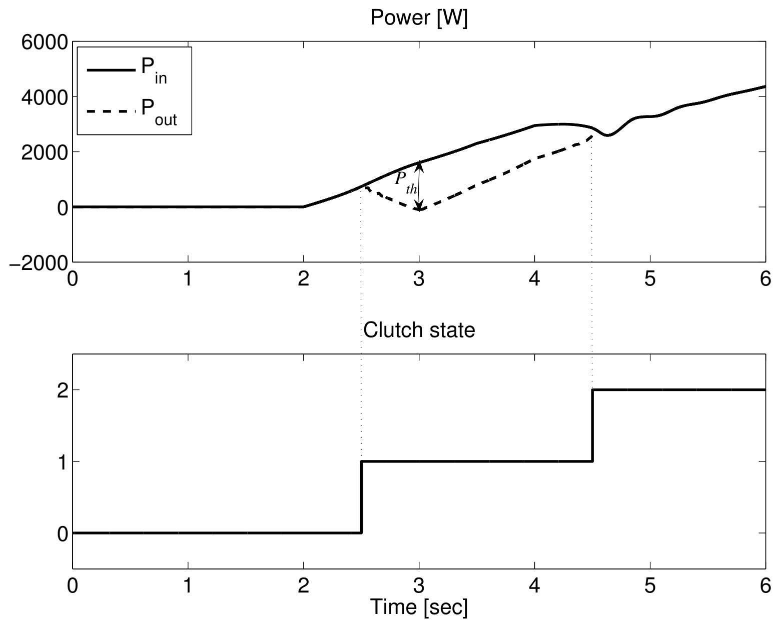

Figure 19: The conservation of power in the clutch.

4 The reduced–order hybrid model $\mathcal{H}_m$

In this section the reduced–order hybrid model of the driveline, referred to as $\mathcal{H}_m$, is described. In the hybrid model $\mathcal{H}_m$ the driveline is represented as two inertias (the crankshaft and the body vehicle) connected by an elasticity, a gear and a clutch (see Figure 20).

In the hybrid model $\mathcal{H}_m$ the clutch model is similar to that shown in Section

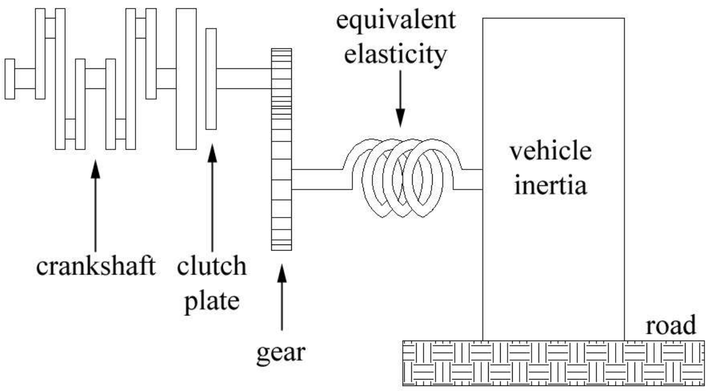

Figure 20: Scheme of the reduced–order hybrid model $\mathcal{H}_m$.

2.2. Differently from the detailed model, when the clutch is in the discrete state *Close*, the whole driveline is represented as a third–order linear system that is very suitable for the synthesis of controllers/observers.

4.1 Crankshaft and flywheel reduced–order model

Similarly to the section 2.1, the crankshaft and the flywheel is modelled as an only rigid inertia and the friction torque T_{fric} has been linearized on the idle to maximal speed range, for $t_{engine} = 110°C$, with a linear viscous friction. In Figures 21 it is reported the $T_{fric}(\omega, t_{engine} = 110°C)$ and the least square line that approximates it. However, the approximation of T_{fric} with linear viscous friction is not satisfactory especially around to the idle speed. An improvement of the performances is obtained by compensating T_{fric} or by a linearization around to a particular point of work. Anyway, in this document it is assumed that the approximation of T_{fric} with a line of the type $b\omega + T_{offset}$ is sufficient.

Under the previous assumptions, the crankshaft dynamics becomes:

$$T_e = J_e\dot{\omega}_e + \breve{b}_e\omega_e + \breve{T}_{offset} + \breve{T}_{clutch}. \tag{29}$$

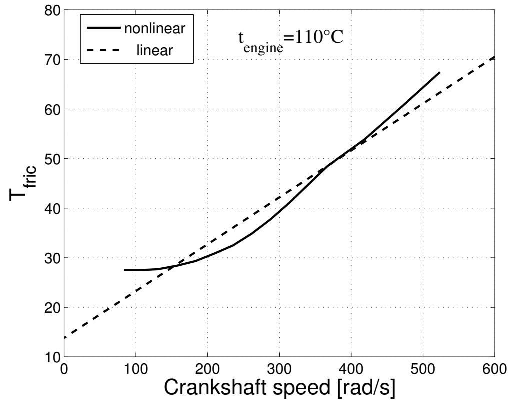

Figure 21: Torque T_{fric} and its least squares approximation line for $t_{engine} = 110°C$.

4.2 Clutch plate reduced–order model

In the hybrid model $\mathcal{H}_m$ the clutch is modelled as described in the Section 2.2, see Figure 8. The coefficient of cinematic friction has been considered constant and equal to $\breve{\mu}_d$. Recall that the maximal transmitted torque for which the clutch remains locked is expressed as in (3), i.e.

$$\breve{T}^{max}_{clutch} = \mu_s n_s \frac{2\pi}{3} \frac{R^3_{ext} - R^3_{int}}{3} P_{clutch}. \tag{30}$$

The torque transmitted in the state *Close* is (see equation 4):

$$\breve{T}_{clutch} = (T_e - \breve{b}_e \omega_e - \breve{T}_{offset}) \frac{\breve{J}_{clutch}}{\breve{J}_{clutch} + J_e} + T_{load} \frac{J_e}{\breve{J}_{clutch} + J_e}, \tag{31}$$

where T_{load} is the torque transmitted by the gear–box reported at the clutch plate and

$$\breve{J}_{clutch} = J_{clutch} + J_p. \tag{32}$$

When $\breve{T}_{clutch} > \breve{T}^{max}_{clutch}$ the clutch FSM enters the *Slip* state, where the transmitted torque is (see equation 5):

$$\breve{T}_{clutch} = \breve{\mu}_d n_s \frac{2\pi}{3} \frac{R^3_{ext} - R^3_{int}}{3} P_{clutch} sign(\omega_e - \omega_{clutch}). \tag{33}$$

If $\omega_e = \omega_{clutch}$ and $\breve{T}_{clutch} \leq \breve{T}^{max}_{clutch}$, then the clutch returns in the state *Close*, while if $P_{clutch} = 0$ the clutch enters in the state *Open* where $\breve{T}_{clutch} = 0$. The dynamics of the clutch plate is:

$$\breve{T}_{clutch} - T_{load} = \breve{J}_{clutch} \dot{\omega}_{clutch} + B_p \omega_{clutch}. \tag{34}$$

4.3 Gear–box reduced–order model

Analogously to the Section 2.5, the gear–box is modelled as a switching system whose FSM is depicted in Figure 13. The inertias and the viscous frictions of the differential, the primary and secondary axis are neglected and the elasticity of the whole driveline is modelled with a single linear elasticity.

When the i-th gear is engaged, the gear–box dynamics is:

$$\begin{aligned} \dot{\alpha}_t &= \tau_i \tau_{diff} \omega_{clutch} - \omega_v \\ \breve{T}_{sma} &= \breve{k}_i \alpha_t + \breve{b}_i (\tau_i \tau_{diff} \omega_{clutch} - \omega_v) \\ T_{load} &= \tau_i \tau_{diff} \breve{T}_{sma} \end{aligned} \tag{35}$$

With neutral gear, the clutch plate and the vehicle inertia are decoupled and the gear–box dynamics is:

$$\begin{aligned} \dot{\alpha}_t &= -1 \\ \breve{T}_{sma} &= 0 \\ T_{load} &= 0 \end{aligned} \tag{36}$$

The elasticity coefficients k_i are obtained analytically from the detailed hybrid model $\mathcal{H}_M$. Firstly, the static characteristic of the clutch of Figure 10 is approximated with a least square line $K_{clutch}\alpha$ (see Figure 22); then, it is assumed that the engine suspensions are rigid. By defining the operator:

$$a//b = \frac{a * b}{a + b} \tag{37}$$

the elasticity k_i with the i–th gear engaged becomes[9]:

$$\begin{aligned} k1 &= k_{lin}//k_{sma} \\ k2 &= \frac{1}{\tau^2}(k_p//K_{clutch}) \\ k_i &= k1//k2. \end{aligned} \tag{38}$$

The damping coefficients b_i, instead, have not been identified analytically but obtained from the time response.

4.4 Vehicle body reduced–order model

The vehicle body in the hybrid model $\mathcal{H}_m$ is modelled as a first–order system with inertia $\breve{J}_v$ and inputs: the torque $\breve{T}_{sma}$ transmitted by the gear–box, the

[9]It is worthwhile to note that the given formulas are obtained under the assumption that it is possible to make permutations between inertias and elasticities. This assumption produces good approximations when the gear–box and semi–axle inertias are much smaller than the crankshaft and vehicle ones.

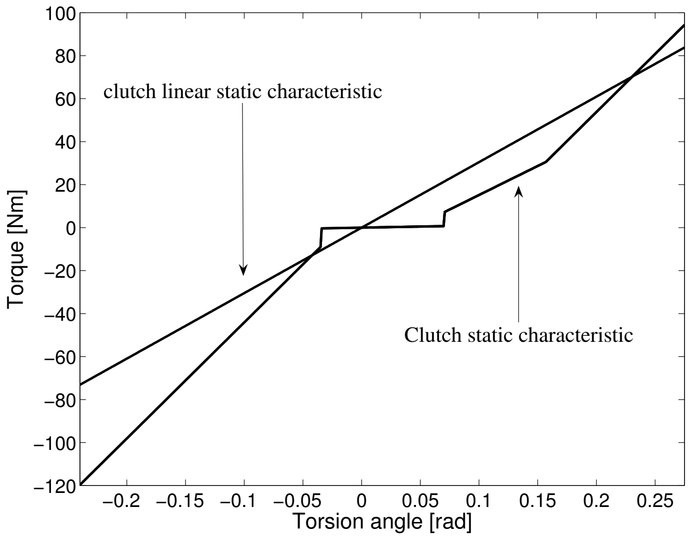

Figure 22: Static characteristic of torsion of the clutch springs and its linearization.

torque T_{slope} due to the slope of the road, the aerodynamics friction T_{air} and the linear viscous friction of the bearing $\breve{b}_v \omega_v$, i.e.

$$\breve{T}_{sma} - T_{slope} - T_{air} - \breve{b}_v \omega_v = \breve{J}_v \dot{\omega}_v \tag{39}$$

where T_{slope} and T_{air} have the same expression of the equation (26) and[8]:

$$\breve{J}_v = J_v + J_w + J_d + \frac{J_s}{\tau_{diff}^2} \tag{40}$$

$$\breve{b}_v = b_w + b_d + \frac{J_s}{\tau_{diff}^2}. \tag{41}$$

4.5 State-space representation of the reduced–order hybrid model $\mathcal{H}_m$

When the clutch is in the discrete state *Close*, the driveline is described as a third–order linear system whose state x comprises the torsion angle α_t, the crankshaft speed ω_e and the wheel speed ω_v. Measurable outputs of the system y are ω_e and ω_v, since they are typically measured by the ECU and the ABS in conventional cars. The input u has two components:

- (i) the average torque engine T_e minus the $\breve{T}_{offset}$;

- (ii) the slope torque T_{slope} plus the torque T_{air} and T_{brake}.

The state-space representation, when the clutch is in the discrete state *Close*, is

$$\dot{x} = \begin{pmatrix} \dot{\alpha}_t \\ \dot{\omega}_e \\ \dot{\omega}_v \end{pmatrix} = A_i \begin{pmatrix} \alpha_t \\ \omega_e \\ \omega_v \end{pmatrix} + B_i \begin{pmatrix} T_e - \breve{T}_{offset} \\ T_{slope} + T_{air} + T_{brake} \end{pmatrix} \tag{42}$$

$$y = Cx \tag{43}$$

where:

$$A_i = \begin{pmatrix} 0 & \tau_i \tau_{diff} & -1 \\ -\frac{\tau_i \tau_{diff} k_i}{J_e + \breve{J}_{clutch}} & -\frac{(\breve{b}_e + B_p) - (\tau_i \tau_{diff})^2 \breve{b}_i}{J_e + \breve{J}_{clytch}} & \frac{\tau_i \tau_{diff} \breve{b}_i}{J_e + \breve{J}_{clutch}} \\ \frac{k_i}{\breve{J}_v} & \frac{\tau_i \tau_{diff} \breve{b}_i}{\breve{J}_v} & -\frac{\breve{b}_i + \breve{b}_v}{\breve{J}_v} \end{pmatrix} \tag{44}$$

$$B_i = \begin{pmatrix} 0 & 0 \\ \frac{1}{J_e + \breve{J}_{clutch}} & 0 \\ 0 & -\frac{1}{\breve{J}_v} \end{pmatrix} \qquad C = \begin{pmatrix} 0 & 1 & 0 \\ 0 & 0 & 1 \end{pmatrix} \tag{45}$$

4.6 Comparison between the models $\mathcal{H}_m$ and $\mathcal{H}_M$

Figure 23 reports a comparison between the crankshaft revolution speed of the hybrid model $\mathcal{H}_m$ and $\mathcal{H}_M$. Notable differences in evolutions are due to a non satisfactory accuracy in considering T_{fric} as linear. Figure 23 (A) and (B) report the crankshaft speed and the discrete state of the clutch during, respectively, a vehicle start-up from stop and a gear shifting from the second to the third gear. In spite of the strong reduction of the hybrid model $\mathcal{H}_m$, the time spent in sliding and closing state of the clutch are nearly the same. In Figure 23 (C) it is shown the evolution of the crankshaft speed of the model $\mathcal{H}_m$ during a sequence of tip–in and tip–out: the model is able to represent the driveline most significant oscillations.

Remark 4.6.1 *As shown in the previous sections, the reduced–order hybrid model $\mathcal{H}_m$ is obtained from the detailed $\mathcal{H}_M$ by swapping between the inertias and the elasticities[8]. In this way the error during transients between the hybrid model $\mathcal{H}_m$ and the hybrid model $\mathcal{H}_M$ is not negligible but it remains always smaller than the error produced under the hypothesis of rigid engine suspensions, absence of backlash and linear clutch springs. However, since the inertias and the frictions of the gear–box have been merged with those of the clutch plate and the vehicle body, the behavior during the steady–state matches that of $\mathcal{H}_M$.*

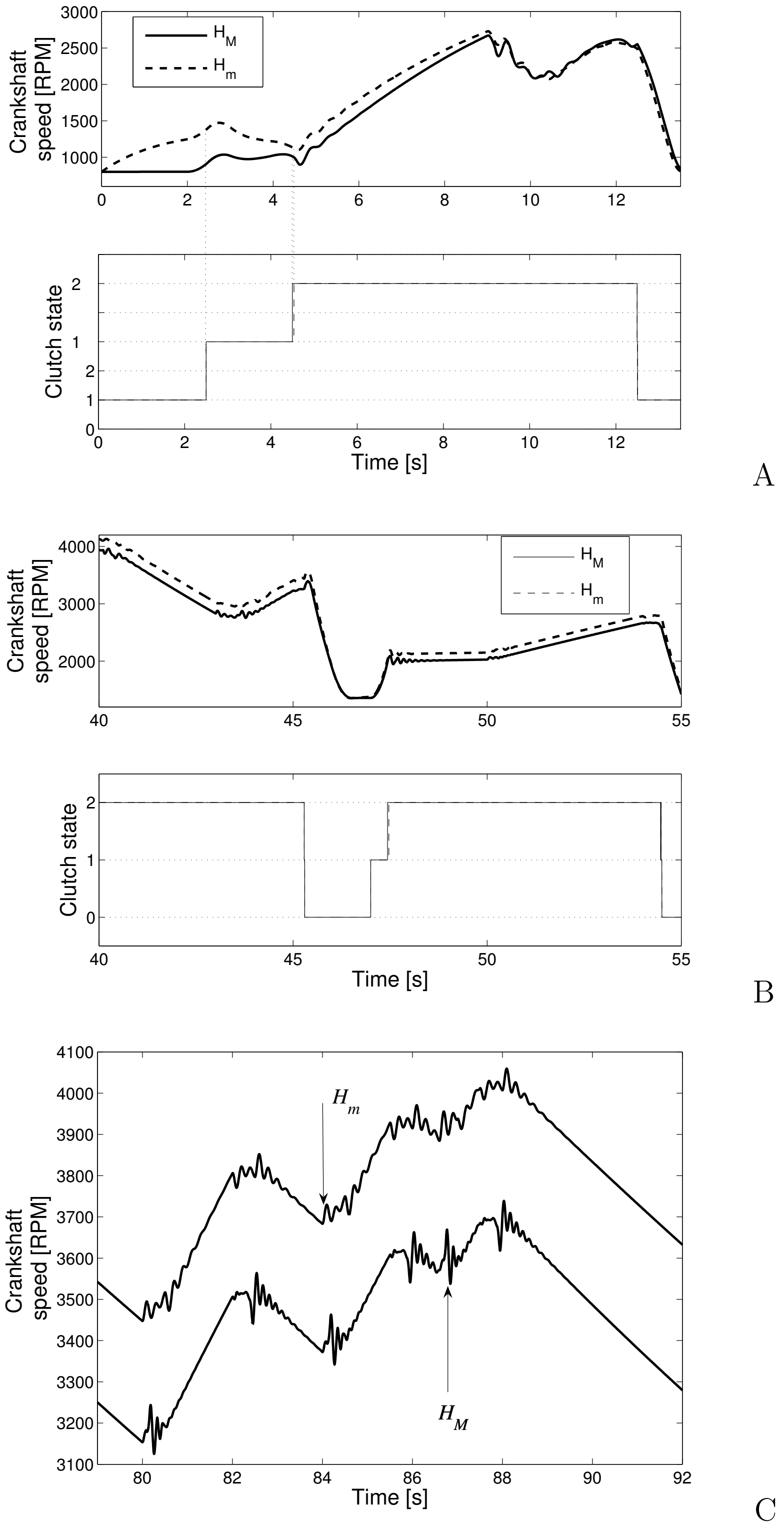

Figure 23: Comparison between the engine speed of the hybrid models $\mathcal{H}_M$ and $\mathcal{H}_m$.

5 Nomenclature.

Symbol	Description	Unit
A	Frontal area of vehicle	m^2
b_{sma}	Coeff. of damping of the semi–axle	$N \cdot m \cdot s/rad$
b_t	Coeff. of damping of the tire	$N \cdot m \cdot s/rad$
b_w	Coeff. of viscosity of the hub	$N \cdot m \cdot s/rad$
$\hat{B}$	Equiv. viscosity of the secondary axle and diff.	$N \cdot m \cdot s/rad$
B_{fi}	Coeff. of damping of the i-th clutch spring	$N \cdot m \cdot s/rad$
B_d	Coeff. of viscosity of the differential	$N \cdot m \cdot s/rad$
B_{high}	High coeff. of damping of the engine suspension	$N \cdot m \cdot s/rad$
B_{low}	Low coeff. of damping of the engine suspension	$N \cdot m \cdot s/rad$
B_p	Coeff. of viscosity of the primary axle	$N \cdot m \cdot s/rad$
B_{ps}	Coeff. of damping of the primary axle	$N \cdot m \cdot s/rad$
B_s	Coeff. of viscosity of the secondary axle	$N \cdot m \cdot s/rad$
$Constant$	Constant rolling friction of the tire	$N \cdot m$
C_x	Drag cefficients	$\frac{N \cdot s^2 \cdot m^2}{Kg \cdot rad^2}$
F_{opt}	Optimal traction force	N
g	Acceleration of gravity	m/s^2
$\hat{J}$	Equiv. inertia of the secondary axle and diff.	$Kg \cdot m^2$
J_b	Cylinder block inertia	$Kg \cdot m^2$
J_{clutch}	Clutch plate inertia	$Kg \cdot m^2$
J_d	Differential inertia	$Kg \cdot m^2$
J_e	Crankshaft–flywheel inertia	$Kg \cdot m^2$
J_p	Primary axle inertia	$Kg \cdot m^2$
J_s	Secondary axle inertia	$Kg \cdot m^2$
J_v	Vehicle inertia	$Kg \cdot m^2$
J_w	Wheel group inertia	$Kg \cdot m^2$

Symbol	Description	Unit
k_{high}	High coeff. of elasticity of the engine suspensions	$N \cdot m/rad$
k_{hyst}	Hysteresis coeff. of elasticity of the tire	$N \cdot m/rad$
k_l	Coeff. of elasticity of the left semi–axle	$N \cdot m/rad$
k_{lin}	Linear coeff. of elasticity of the tire	$N \cdot m/rad$
k_{low}	Low coeff. of elasticity of the engine suspensions	$N \cdot m/rad$
k_p	Coeff. of elasticity of the primary axle	$N \cdot m/rad$
k_r	Coeff. of elasticity of the right semi–axle	$N \cdot m/rad$
k_{sma}	Coeff. of elasticity of the semi–axle	$N \cdot m/rad$
K_{fi}	Coeff. of elasticity of the i-th clutch spring	$N \cdot m/rad$
M_v	Vehicle mass	Kg
n_s	Number of friction surface	[ ]
P	Power engine at the wheels	W
P_{in}	Power at the input of the crankshaft	W
P_{clutch}	Clutch plate pressure	N/m^2
$P_{J_{clutch}}$	Accelerative power for the J_{clutch} inertia	W
P_{J_e}	Accelerative power for the J_e inertia	W
P_{out}	Power at the output of the clutch	W
$P_{springs}$	Power transmitted by the clutch springs	W
P_{th}	Thermal power losses during the slip	W
$P_{\%}$	Road slope	%
R_{eff}	Effective radius of the tire	m
R_{ext}	External radius of the clutch	m
R_{int}	Internal radius of the clutch	m
t_{engine}	Engine temperature	$^{\circ}C$
T_{brake}	Brake torque	$N \cdot m$
T_{clutch}	Torque transmitted by the clutch	$N \cdot m$
T_{clutch}^{max}	Torque capacity of the clutch	$N \cdot m$
T_{air}	Aerodynamics friction	$N \cdot m$
T_e	Average torque engine	$N \cdot m$
T_{fric}	Friction torque on the crankshaft	$N \cdot m$
T_{roll}	Rolling friction of the tire	$N \cdot m$
T_{slope}	Slope road torque	$N \cdot m$
T_{sma}	Torque transmitted by the semi–axle	$N \cdot m$
$T_{springs}$	Torque transmitted by the clutch springs	$N \cdot m$
$T_{springs}^{i}$	Torque offset of the i-th clutch springs	$N \cdot m$
T_{susp}	Torque transmitted by the engine suspensions	$N \cdot m$
$\hat{T}_{tire}$	Torque transmitted by the tire on the hub side	$N \cdot m$
T_{tire}	Torque transmitted by the tire on the vehicle side	$N \cdot m$
T_0	Torque offset of the tire	$N \cdot m$
v	Vehicle speed	m/s

Symbol	Description	Unit
α	Backlash angle	rad
α_b	Torsion angle of the engine suspension	rad
α_{diff}	Differential angle	rad
α_l	Hysteresis angle of the tire	rad
α_p	Torsion angle of the primary axle	rad
$\alpha_{springs}$	Torsion angle of the clutch springs	rad
α_{tire}	Torsion angle of the tire	rad
α_w	Wheel angle	rad
α_0	Reversal angle of the tire	rad
α_0^i	Discontinuity angle of the i-th clutch springs	rad
α_1	Discontinuity angle of the engine suspension	rad
μ_d	Kinetic coefficient of friction of the clutch	[ ]
μ_s	Static coefficient of friction of the clutch	[ ]
ρ	Density of the air	Kg/m^3
τ_{diff}	Transmission ratio of the differential	[ ]
τ_i	Transmission ratio of the i-th gear	[ ]
ω_b	Cylinder block speed	rad/s
ω_{diff}	Differential speed	rad/s
ω_e	Crankshaft speed	rad/s
ω_{clutch}	Clutch plate speed	rad/s
ω_p	Primary axle speed	rad/s
$\omega_{vehicle}$	Vehicle speed	rad/s
ω_w	Wheel group speed	rad/s

Abbreviation	Explanation	Unit
A_i, B_i, C	Matrix of the state-space representation	–
$\breve{b}_i$	Coeff. of damping of the driveline with i-th gear	$N \cdot m \cdot s/rad$
$\breve{b}_e$	Linear term of the friction torque on the crankshaft	$N \cdot m \cdot s/rad$
$\breve{k}_i$	Coeff. of elasticity of the driveline with i-th gear	$N \cdot m/rad$
$\breve{T}_{clutch}^{max}$	Torque capacity of the clutch	$N \cdot m$
$\breve{T}_{clutch}$	Torque transmitted by the clutch	$N \cdot m$
T_{load}	The torque T_{sma} reported at the clutch plate	$N \cdot m$
$\breve{T}_{sma}$	Torque transmitted by the gear–box to the vehicle	$N \cdot m$
$\breve{T}_{offset}$	Offset term of the friction torque on the crankshaft	$N \cdot m$
$\breve{J}_{clutch}$	Equivalent clutch plate inertia	$Kg \cdot m^2$
$\breve{J}_v$	Equivalent vehicle inertia	$Kg \cdot m^2$
α_t	Torsion angle of the driveline	rad
$\breve{\mu}_d$	Constant kinetic coefficient of friction of the clutch	[ ]
ω_v	Vehicle speed	rad/sec

Abbreviation	Explanation
ABS	Anti–lock Brake System
CVT	Continuous Variable Transmission
DMF	Dual Mass Flywheel
ECU	Electronic Control Unit
FFT	Fast Fourier Transform
FSM	Finite State Machine
$\mathcal{H}_m$	Reduced–order hybrid model of driveline
$\mathcal{H}_M$	Detailed hybrid model of driveline
IC	Internal Combustion engine
VDV	Vibration Dose Value

References

[1] ASM Handbook Volume 18: Friction, Lubrication and Wear Technology. *ASM International*, 1992

[2] J. Baumann, D.D. Torkzadeh, A. Ramstein, U. Kiencke, T. Schlegl. Model–Based Predictive Anti–Jerk Control. *IFAC Symposium "Advances in Automotive Contyrol"*, 2004.

[3] M. Bodden, R. Heinrichs. Analisys of the Time Structure of Gear Rattle. *Internal Technical Report*, 1999.

[4] Automotive Handbook. *Bosch* 4th Edition 1996.

[5] A. Balluchi, L. Benvenuti, C. Lemma, A.L. Sangiovanni–Vincentelli, G. Serra. Actual Engaged Gear Identification: a Hybrid Observer Approach. To appear at *16th IFAC World Congress*, 2004.

[6] A. Balluchi, L. Benvenuti, M.D. Di Benedetto, C. Pinello, and A.L. Sangiovanni–Vincentelli, "Automotive Engine Control and Hybrid Systems: Challenges and Opportunities", *Proceedings of the IEEE* Special Issue on Hybrid Systems (invited paper) 88(7) 2000, 888-912.

[7] A. Beydounl, L.Y. Wang. Coordinaltion of Engine and Transmission Using Hybrid Control Methodologies. *Proceedings of the American Control Conference*, Philadelphia, Pennsylvania, 1998.

[8] N. Cavina, G. Serra. Analysis of a Dual Mass Flywheel System for Engine Control Applications. *SAE Technical Paper* 2004-01-3016.

[9] S. N. Dogan. Loose part vibration in vehicle transmissions - Gear rattle. *Tr. J. of Engineering and Environmental Science* 23 (1999) , 439–454

[10] A. Farshidianfar, M. Ebrahimi, H. Bartlett. Hybrid modelling and simulation of the torsional vibration of vehicle driveline systems. *Proc. Instn Mech Engrs*, Vol. 215, Part. D, 2001

[11] F. Garofalo, L. Glielmo, L. Iannelli, F. Vasca. Smooth Engagement for Automotive Dry Clutch. *Proceedings of the 40th IEEE Conference on Decision and Control.* Orlando, Florida, USA, 2001.

[12] T.D. Gillespie. Fundamentals of Vehicle Dynamics. *SAE International* 1992.

[13] M.J. Griffin. Handbook of human vibration, *Academic Press*, London, 1990.

[14] S. Johansson, E. Langjord, S. Pettersson. Objective Evaluation of Shunt and Shuffle in Vehicle Powertrains. *International Symposium on Advanced Vehicle Control* (AVEC 04), 2004.

[15] S. Johansson. Shunt and Shuffle Evaluation for Vehicle Powertrains. Master Thesis, Chalmers University of Technology, Mechanical Department, 2004.

[16] J. Karlsson. Powertrain Modeling and Control for Driveability in Rapid Transients. *Laurea Thesis*, Machine and Vehicle Design, Chalmers University of Technology Gteborg, Sweden 2001.

[17] A. Lamberberg, B. Egardt. Estimation of Backlash in Automotive Powertrain – An Experimental Validation. *IFAC Symposium "Advances in Automotive Contyrol"*, 2004.

[18] A. Lamberberg. A literature survey on control of automotive powertrains with backlash. *Technical Report R013/2001.* Control and Automation Laboratory, Department of Signals and Systems, Chalmers University of Technology, 2001.

[19] A. Lamberberg, B. Egardt. Evaluation of control strategies for automotive powertrains with backlash. *International Symposium on Advanced Vehicle Control* (AVEC 02), 2002.

[20] S. Meisner, B. Campbell. Development of Gear Rattle Analytical Simulation Methodology. *SAE Technical Report 951317.*

[21] M. T. Menday, H. Rahnejat, M. Ebrahimi. Clonk: an onomatopoeic response in torsional impact of automotive drivelines, *Journal of Automotive Engineering*, vol 213, no D4, 1999

[22] C.Y. Mo, A.J. Beaumont, N.N. Powell. Active control of driveability. *SAE Technical Report 960046* , 1996

[23] R. Morselli, R. Zanasi, A. Visconti. Generation of Acceleration Profiles for Smooth Gear Shift Operations. *IEEE Transaction on Control System Technoilogy*

[24] M. Petterson. Driveline Modeling and Principles for Speed Control and Gear-Shift Control. *Laurea Thesis No.564, 1996*, Department of Electrical Engineering, Division of Vehicular Systems, Linkoping University, S-581 83 Linkoping, Sweden.

[25] M. Petterson, L. Nielsen, L.G. Hedstr. Trasmission-torque control for gear shifting with engine control. *SAE Technical Report 979864*, 1997

[26] M. Pettersson, L. Nielsen. Gear Shifting by Engine Control. *IEEE Trransactions On Control Systems Technology*, Vol.8, No.3, 2000.

[27] W. Reik, R. Seebacher, A. Kooy. Dual Mass Flywheel. *6th International Symposium, Baden- Baden: LuK Buhl*, 1998, pp. 69-94.

[28] S. De La Salle, M. A. Janz, D.A. Light. Design of a feedback control system for damping of vehicle shuffle. *EAEC European Automotive Congress.* Barcelona, Spain, 1999.

[29] A. Schwenger, M. Henn, U. Hinrichsen, H. Haase. Active Damping of Driveline Oscillation. *IFAC Symposium "Advances in Automotive Contyrol"*, 2004.

[30] J.M. Slicker, R.N.K. Loh. Design of Robust Vehicle Launch Control System. *IEEE Transaction on Control System Technology*, Vol.4, No.4, 326:335, 1996.

[31] A. G. Stefanopoulou et al. Modeling and Control of a Spark Ignition Engine with Variable Cam Timing, *Proceedings of the American Conference*, Seattle, Washington, June, 1995.

[32] P. Stewart, P.J. Fleming. Drive-by-Wire Control of Automotive Driveline Oscillations by Response Surface Methodology. *IEEE Transactions On Control Systems Technology*, Vol.12, No. 5, 2004.

[33] J. R. Zachary, A. M. Scott, and J. J. Moskwa. Development of the Automotive Research Center (ARC), Powertrain System Dynamic Models, 1997 *Spring Technical Conference*, ASME, Paper No. ICE-Vol. 28-1, 1997.

[34] J.C. Zavala, P.Stewart, P.J. Fleming. Multiobjective Automotive Drive By Ware Controller Design. *IEEE International Symposium on Computer Aided Control System Design Proceedings*, 69:73, Glasgow, Scotland, U.K.